Lehrstuhl für Bildverarbeitung
Institute of Imaging & Computer Vision

Modeling and Compensation of Ghosting in Multispectral Filter Wheel Cameras

Johannes Brauers and Til Aach
Institute of Imaging and Computer Vision
RWTH Aachen University, 52056 Aachen, Germany
tel: +49 241 80 27860, fax: +49 241 80 22200
web: www.lfb.rwth-aachen.de

in: IEEE Southwest Symposium on Image Analysis and Interpretation. See also BibTeX entry below.

BibTeX:

```
@inproceedings{Brauers2008b,
  author      = {Johannes Brauers and Til Aach},
  title       = {Modeling and Compensation of Ghosting in Multispectral Filter Wheel Cameras},
  booktitle   = {IEEE Southwest Symposium on Image Analysis and Interpretation},
  year        = {2008},
  month       = {Mar},
  day         = {24-26},
  address     = {Santa Fe, New Mexico, USA},
}
```


document created on: December 2, 2008
created from file: paper.tex
cover page automatically created with CoverPage.sty
(available at your favourite CTAN mirror)

RWTH AACHEN
RHEINISCH-WESTFÄLISCHE TECHNISCHE HOCHSCHULE AACHEN

Modeling and Compensation of Ghosting in Multispectral Filter Wheel Cameras

Johannes Brauers and Til Aach
RWTH Aachen University
Institute of Imaging & Computer Vision
D-52056 Aachen, Germany
email: jb,ta@lfb.rwth-aachen.de

Abstract

Multispectral filter wheel cameras divide the visible electromagnetic spectrum by using several optical bandpass filters mounted on a filter wheel and acquire one color component for each filter wheel position. Afterwards, the single images are combined into one multispectral image. While the color accuracy of this approach and the stop-band attenuation of the bandpass filters is superior to other technologies, ghosting images are produced by reflections between the image sensor and the filter surface: The original image is duplicated in a displaced, weaker and softened form and added to the original image, thus compromising the original. We analyze the path of rays in this specific optical setup and derive a physical model for the ghosting reflections. By linking the physical model to the image content, we derive a calibration and compensation algorithm, whose parameters are estimated from a test image. Application of our correction algorithm makes the ghosting virtually vanish.

1 Introduction

Conventional 1-chip RGB imaging sensors built into mobile phones up to professional cameras provide the basis for cheap, robust and mass-produced cameras. In most cases the users are satisfied with their color reproduction, although they exhibit a systematic color error [9] and require interpolation algorithms [5] to reconstruct the full color information. The color errors are caused by violation of the Luther rule [10], which states that the spectral sensitivities of the sensor have to be a linear combination of the CIE observer's ones.

In contrast, multispectral cameras mostly fulfill the Luther rule because they sample the spectrum at a higher number of equidistant intervals. One prominent representative is the filter wheel camera [7], using optical bandpass filters between lens and imaging sensor as shown in Fig. 1: A certain wavelength range of the spectrum passes through an optical narrow-band filter and is acquired by the gray level sensor. By rotating the filter wheel, several color channels are acquired successively and are finally combined into one multispectral color image.

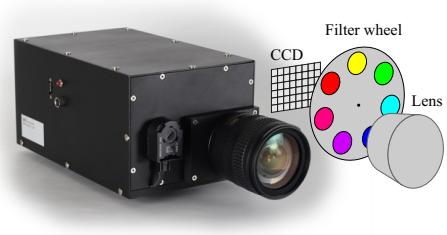

Figure 1. Our multispectral camera with its internal configuration sketched.

Another technology for acquisition of multispectral images uses *one* liquid crystal tunable filter (LCTF) [1] instead of the optical bandpass filters, where the spectrum of the filter can be electronically tuned. While it is superior to bandpass filter wheels in terms of size and mechanical components, the liquid crystal is highly temperature-dependent and does not provide the excellent stop-band attenuation of optical filter glass.

However, optical bandpass filter glasses are highly reflective and – together with the similarly reflective CCD sensor – cause a duplicate image shown in Fig. 2. Because it is practically unfeasible to align the optical bandpass filters in a fully coplanar manner, the ghosting duplicate is shifted relative to the original image. Furthermore, the ghosting effect is hardly noticeable in a normal image since the reflection's amplitude is approximately 1% of the original image amplitude. But when using high dynamic range imaging (HDRI) [3], where the image might be rescaled to amplify the dark regions, the ghosting artifacts get clearly visible.

In [6], a method for "Compensating for Stray Light" is

presented. However, since the author uses a low frequency model for compensation while our ghosting artifacts are rather sharp, the proposed method will not work in our case. The approach introduced in [8] models stray light by using a complex position-dependent PSF, but does not describe the derivation of the PSF. Both papers do not model the optical path in the camera and therefore derive rather heuristic models. Here, we analyze the optical setup first, in order to provide a base for our model.

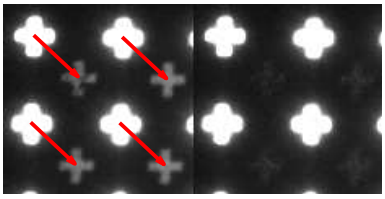

Figure 2. Ghosting effect (left) and compensation (right) (brightened five-fold).

We start with a description of the physical causes of the ghosting effects and derive a corresponding model in section 2. Based on this model, we present a calibration and compensation algorithm in section 3. Results of this algorithm are given in section 4 before we finish with conclusions.

2 Physical Model

Fig. 4 shows our optical setup and raytracing results: The incoming rays from the object on the left side pass through the aperture and lens and impinge on the tilted filter glass. They are refracted when entering the filter glass as well as when leaving the filter glass. Because the refraction indices are fixed, the rays leave the filter with a parallel offset. We already developed a mathematical model for the distortions caused by the filter glass in [2].

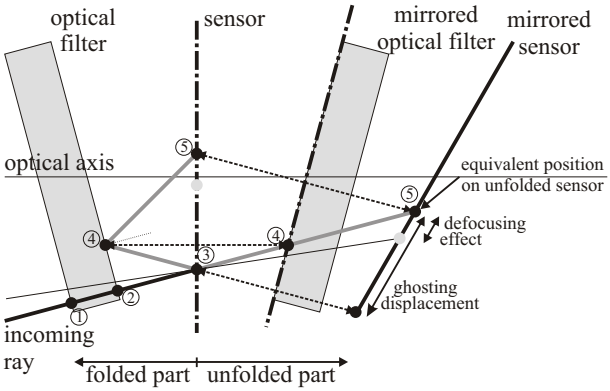

Figure 3. Folded and unfolded model.

Details of the reflections between sensor and optical filter are depicted in Fig. 3 (left half): When the ray leaves the filter ②, it impinges on the imaging sensor at ③ and produces the original image without ghosting artifacts. But since the imaging sensor has a highly reflective surface, the ray is also partly reflected and directed back to the filter surface, where it is reflected once more ④. The ghosting image is generated when the twice-reflected ray impinges on the imaging sensor the second time at ⑤. Although there might be an unlimited number of reflections, we only consider 1st order reflections since the attenuation is quite high and the size of the sensor is limited.

To simplify the model, we develop an equivalent model by mirroring all components including the ray instead of the ray itself: As shown in the right half of Fig. 3 termed *unfolded part*, the optical filter glass on the left side of the imaging sensor is mirrored by taking the sensor as the symmetry axis. By doing so, the path of the ray ③-④ is also mirrored and becomes virtually a straight extension of the previous section ②-③. The optical filter is also shown on the right side of the sensor, although it has no effect, since the ray is reflected on its surface near to the sensor. Now the mirror procedure is repeated and the sensor itself is mirrored by the virtual optical filter on the right half of the figure. This equivalent model can be verified by mirroring the points ④-⑤ at their corresponding mirror axes. The correspondences are marked with dotted lines in the figure.

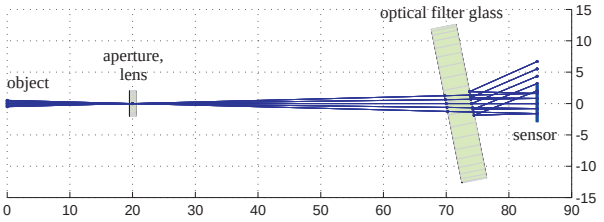

Figure 4. Raytracing results for our optical system.

From the model in Fig. 3 we derive that points arriving at the CCD at position ③ appear a second time at position ⑤, causing the ghosting artifacts. The unfolded model in the figure gives an intuitive understanding of this phenomenon and enables the derivation of a model with three key issues: First, the imaging sensor and the optical filter do not exhibit a 100% reflectivity but a certain reflection factor $r \ll 1$. Secondly, the reflection does not appear at the same position as the original ray since the filter glass is tilted. From the unfolded model we derive that the ghosting image is a *projection* of the original image: Both sensors, the original one and the mirrored one, may be considered as screens the images are projected onto. Since the right screen is tilted, the ghosting image is distorted. Thirdly, the ghosting image is defocused because the effective image distance is increased, i.e., the virtual sensor is not in the focus plane. In Fig. 3, the thin ray may illustrate the defocusing: While it

appears at the same position on the original sensor as the thick ray, due to its different incident angle at position ③ it impinges on the virtual sensor at another position. The defocusing may be modeled by a point spread function (PSF). Measurements show that it suffices to assume a fixed PSF for the complete image.

The ghosting effect can be mathematically modeled by

$$g(x,y) = f(x,y) + r f(x',y') * h(x,y)\ , \qquad (1)$$

with

$$\begin{pmatrix} u & v & w \end{pmatrix}^T = \mathbf{M} \begin{pmatrix} x & y & 1 \end{pmatrix}^T \qquad (2)$$

and

$$x' = \frac{u}{w} \quad y' = \frac{v}{w}\ . \qquad (3)$$

The term $g(x,y)$ describes the acquired camera image, $f(x,y)$ the original image without ghosting, r the reflection factor, and $h(x,y)$ the blurring PSF. The distortion of the ghosting image compared to the original image is modeled by a projective mapping [4] of the image coordinates according to (2). The matrix $\mathbf{M}$ is a 3×3 matrix describing the projective transform and will be estimated from sample point pairs with a pseudoinverse. We assume the blurring PSF $h(x,y)$ to be a Gaussian blur kernel with a standard deviation σ.

3 Calibration and Correction Algorithm

The basis of our calibration algorithm is the acquisition of a backlit slide (see Fig. 6) with several transparent crosses on it. We use high dynamic range imaging (HDRI) [3] to recover details in the bright crosses as well as the dark surrounding regions, where the ghosting artifacts are detected. The left half of Fig. 2 shows an acquired image, which has been brightened five-fold to highlight the ghosting artifacts. Our aim is to compute the displacement vectors between original cross symbols and the corresponding ghosting artifacts shown in the figure, and to derive the parameters of Eq. (1)-(2), namely the reflection factor r, the parameter of the blurring kernel σ and the transformation matrix $\mathbf{M}$.

An overview of our calibration algorithm is given in Fig. 5: First, our special calibration image allows us to split the image virtually perfectly into the original and ghosting image by applying a threshold, which is computed from the maximum of the original image. While in most cases, this is not possible for *normal* images, for our test image it works perfectly. Our next step is the computation of the displacements between each cross image and its corresponding ghosting image as shown in Fig. 2 by vector arrows. Towards this end, we initialize the registration by determining the position of each cross with connected component labeling and compute the center of gravity for each symbol. To restrict the search space of the following fine registration, we compute the global displacement between original and ghosting. This results only in a rough estimation since the real model given in (1) is position dependent. The displacement estimation is carried out by using normalized cross correlation – the maximum correlation then marks the displacement offset. The estimated rough global displacement is taken as a starting vector for the refined template matching, which is performed for each cross individually. At this point, we have estimated a vector field, where each vector corresponds to the displacement between original and ghosting symbol.

From the displacement vector field we then derive the transformation matrix $\mathbf{M}$ of Eq. (2) which describes the geometrical transformation of the original image to the ghosting image. Now we are able to apply the transformation to obtain an artificial ghosting image and compare it to the real ghosting image. The missing parameters r and σ are then computed by minimizing the variance of the corrected image

$$\hat{f}(x,y) = g(x,y) - r f(x',y') * h(x,y) \qquad (4)$$

in the dark regions, i.e. the resulting image is masked to exclude the original symbols, thus showing only the regions with ghosting. For minimization, we use the Nelder-Mead simplex method [11].

Since the parameters have to be estimated only once for a specific optical setup, new images may be directly compensated by applying (4). Only the zoom setting of the lens may influence the parameters.

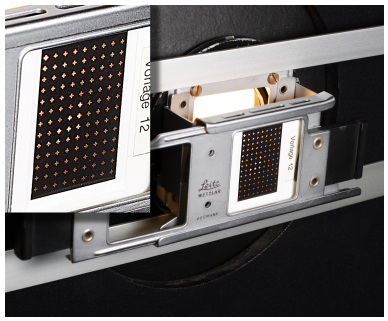

Figure 6. Calibration slide mounted in front of our integrating sphere.

4 Experimental Results

We performed the experiments with our multispectral camera featuring a 7-channel filter wheel shown in Fig. 1. The internal camera Sony XCD-SX900 exhibits a resolution

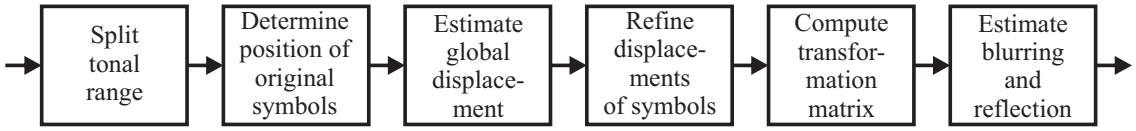

Figure 5. Block diagram of our calibration algorithm.

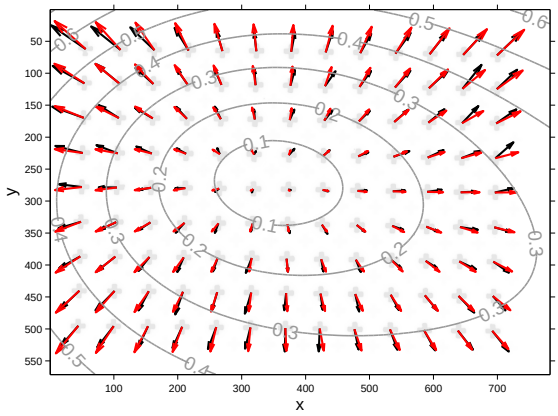

Figure 7. Scaled measured vector field (⟶), mean vector subtracted; model vector field (⟶); numbers denote vector length.

of 1280 × 960 pixels and the chip size is 6.4mm × 4.8mm. The lens is a Nikkor AF-S DX 18-70mm.

We estimated the reflectance factor of our model (1) to $r = 0.0099$, which means that the ghosting effect is approximately 100 times weaker than the original image. In an 8 bit image, the ghosting effect therefore causes an increase of 2.54 values. Although this might sound negligible, when using HDR imaging it can be clearly seen (Fig. 2). The standard deviation of the Gaussian blur was quantified to be $\sigma = 0.54$, and represents a rather conservative smoothing. The transformation matrix was computed to

$$\mathbf{M} = \begin{pmatrix} 1.0017 & 0.0004 & 27.2023 \\ 0.0001 & 1.0023 & 25.3360 \\ 0.0000 & 0.0000 & 1.0000 \end{pmatrix}, \qquad (5)$$

with a mean error of 0.043 pixel and a maximum error of 0.155 pixel between measured and modeled displacement vectors. The upper right elements indicate a rather large displacement of $(\Delta x, \Delta y) = (27.2, 25.3)$ pixels. If the ghosting image were just a shifted version of the original image, the matrix diagonal elements would be exactly one and the off-diagonal elements in the left two columns would be zero. Since this is not the case, there is a superimposed position-dependent vector field shown in Fig. 7. The vector field in the figure has been plotted by previously subtracting the fixed displacement part. It can be seen that the measured (⟶) and the modeled vector field match quite well.

When finally applying the compensation (4), the ghosting practically vanishes (right half of Fig. 2).

5 Conclusions

We have derived a physical model for the ghosting artifacts arising from the reflections between sensor and filter glass surface. We enabled an intuitive understanding of the model by creating a virtual mirrored duplicate of the optical filter and the sensor. Based on this model, we derived a calibration and compensation algorithm, which determines the parameters of our model and is able to compensate the ghosting images. An interesting question is, whether the estimation of the parameters is also possible from *normal* images, instead of the calibration image.

References

[1] Cambridge Research & Instrumentation, Inc.

[2] J. Brauers, N. Schulte, and T. Aach. Modeling and compensation of geometric distortions of multispectral cameras with optical bandpass filter wheels. In *15th EUSIPCO*, Poznań, Poland, Sep 2007.

[3] J. Brauers, N. Schulte, A. A. Bell, and T. Aach. Multispectral high dynamic range imaging. In *IS&T/SPIE EI*, San Jose, California, USA, Jan 2008. Accepted for publication.

[4] D. A. Forsyth and J. Ponce. *Computer Vision: A Modern Approach*. Prentice Hall, August 2002.

[5] B. Gunturk, J. Glotzbach, Y. Altunbasak, R. Schafer, and R. Mersereau. Demosaicking: color filter array interpolation. *IEEE SPM*, 22(1):44–54, January 2005.

[6] S. Helling. Improvement of multispectral image capture by compensating for stray light. In *IS&Ts CGIV*, volume 3, pages 458–462, Leeds, UK, June 2006.

[7] S. Helling, E. Seidel, and W. Biehlig. Algorithms for spectral color stimulus reconstruction with a seven-channel multispectral camera. In *IS&Ts CGIV*, volume 2, pages 254–258, Aachen, Germany, Apr 2004.

[8] P. A. Jansson and R. P. Breault. Correcting color-measurement error caused by stray light in image scanners. In *IS&T/SID CIC*, volume 6, pages 69–73, Scottsdale, Arizona, USA, Nov 1998.

[9] F. König and P. G. Herzog. On the limitation of metameric imaging. *Proc. IS&T´s PICS*, 2:163–168, 1999.

[10] R. Luther. Aus dem Gebiet der Farbreizmetrik. *Zeitschrift für technische Physik*, 8:540–558, 1927.

[11] J. Nelder and R. Mead. A simplex method for function minimization. *Computer Journal*, 7:308–313, 1965.